Mechanism of Oxidatively Induced Migratory Insertion of Carbon Monoxide. Evidence for a 19-Electron Intermediate

Michael J. Therien and William C. Trogler*

Contribution from the Department of Chemistry, D-006, University of California at San Diego, La Jolla, California 92093. *Received August 7, 1986*

Abstract: The mechanism of oxidatively induced CO insertion for $CpFe(CO)(PPh_3)CH_3$ has been probed by transient electrochemical techniques. The data presented herein suggest that the alkyl-to-acyl migration at 17-electron $CpFe(CO)(PPh_3)CH_3^+$ proceeds by a mechanism consisting of two chemical steps. The first step is a second-order process, first order in both the metal radical and entering pyridine nucleophile (Nu), that produced a 19-electron species $CpFe(CO)(PPh_3)(Nu)CH_3^+$. This complex can be observed directly at low temperature in cyclic voltammetry measurements and in the EPR and IR spectra. The rate of nucleophilic attack at $CpFe(CO)(PPh_3)CH_3^+$ depends on the σ-basicity of the nitrogen Lewis base as seen from second-order constants, k_1, that vary over 5000-fold from 200 (3,4-dimethylpyridine) to 0.04 (3-cyanopyridine) M^{-1} s^{-1} at 20 °C. Hammett analysis of the rate data shows that log k_1 correlates well with the σ-meta and σ-para values for eight 3- and 4-substituted pyridines. The second chemical step that occurs is a nucleophile concentration independent first order process that converts the intermediate $CpFe(CO)(PPh_3)(Nu)CH_3^+$ to the acyl product, 17-electron $CpFe(PPh_3)(Nu)(COCH_3)^+$. We rule out a mechanism for the oxidatively induced migratory insertion that proceeds via a 15-electron intermediate, where insertion occurs before nucleophile coordination at $CpFe(CO)(PPh_3)CH_3^+$.

Recent studies of carbonyl-containing 17-electron (17e) organometallic radicals[1-18] have led to speculation that these labile species may function as intermediates in catalytic cycles.[19,20] For example, the reaction between styrene and $HCo(CO)_4$ yields an aldehyde product by a mechanism that involves metal-centered radicals.[16,19,20] Since alkyl-to-acyl migratory insertions represent the cornerstone of many carbonylation processes of industrial importance, we now report a study of this process at a 17e metal center.

Cyclopentadienyl (Cp) iron alkyl carbonyl complexes undergo oxidatively induced carbonyl insertions into metal–alkyl bonds.[18,21] The migratory insertion occurs rapidly and gives a trillionfold increase in the equilibrium constant for insertion in comparison to the neutral 18e parent complexes.[18] Qualitative information from these studies suggests the reaction pathway follows an E_rC_r mechanism (eq 1 and 2)

$$CpFe(CO)(L)CH_3 \underset{E_i}{\overset{E_f}{\rightleftharpoons}} CpFe(CO)(L)CH_3^+ \qquad (1)$$

$$L = PPh_3$$

$$CpFe(L)(COCH_3)^+ \text{ or } CpFe(CO)(L)CH_3^+ + L' \underset{k_b}{\overset{k_f}{\rightleftharpoons}} CpFe(L)(L')C(O)CH_3 \qquad (2)$$

where the species that reacts with L' = acetonitrile may be either a 15e acyl or a 17e alkyl complex.[18] Doxsee et al.[14] have proposed that this reaction involves an intermediate of expanded coordination number. In this paper we present kinetic, electrochemical, and spectroscopic evidence showing that the reactive species for the CO insertion process in these iron–alkyl radicals are 17e or 19e complexes. A key step in the oxidatively induced insertion reaction is nucleophilic attack at the 17e metal center that results

(1) (a) Brown, T. L. *Ann. N.Y. Acad. Sci. U.S.A.* **1980**, *333*, 80. (b) Halpern, J. *Pure Appl. Chem.* **1986**, *58*, 575. (c) Kochi, J. K. *Organometallic Mechanisms and Catalysis*; Academic: New York, 1978. (d) Collman, J. P.; Hegedus, L. S. *Principles and Applications of Organotransition Metal Chemistry*; University Science Books: Mill Valley, CA 1980. (e) Lappert, M. F.; Lednor, P. W. *Adv. Organomet. Chem.* **1976**, *14*, 345. (f) Kochi, J. K. *J. Organomet. Chem.* **1986**, *300*, 139.

(2) Darchen, A.; Mahê, C.; Patin, H. *J. Chem. Soc., Chem. Commun.* **1982**, 243.

(3) (a) Hershberger, J. W.; Kochi, J. K. *J. Chem. Soc., Chem. Commun.* **1982**, 212. (b) Hershberger, J. W.; Klinger, R. J.; Kochi, J. K. *J. Am. Chem. Soc.* **1982**, *104*, 3034. (c) Zizelman, P. M.; Amatore, C.; Kochi, J. K. *Ibid.* **1984**, *106*, 3771.

(4) Kinney, R. J.; Jones, W. D.; Bergman, R. G. *J. Am. Chem. Soc.* **1978**, *100*, 7902.

(5) Schroder, N. C.; Angelici, R. J. *J. Am. Chem. Soc.* **1986**, *108*, 3688.

(6) (a) Stiegman, A. E.; Goldman, A. S.; Leslie, D. B.; Tyler, D. R. *J. Chem. Soc., Chem. Commun.* **1984**, 632. (b) Stiegman, A. E.; Stieglitz, M.; Tyler, D. R. *J. Am. Chem. Soc.* **1983**, *105*, 6032. (c) Goldman, A. S.; Tyler, D. R. *J. Am. Chem. Soc.* **1984**, *106*, 4066. (d) Stiegman, A. E.; Tyler, D. R. *Inorg. Chem.* **1984**, *23*, 527. (e) Stiegman, A. E.; Tyler, D. R. *Acc. Chem. Res.* **1984**, *17*, 61.

(7) (a) Shi, Q.-Z.; Richmond, T. G.; Trogler, W. C.; Basolo, F. *J. Am. Chem. Soc.* **1984**, *106*, 71. (b) Richmond, T. G.; Shi, Q.-Z.; Trogler, W. C.; Basolo, F. *J. Am. Chem. Soc.* **1984**, *106*, 76. (c) Kowaleski, R. M.; Trogler, W. C.; Basolo, F. *Gazz. Chim. Ital.* **1986**, *116*, 105. (d) Kowaleski, R. M.; Basolo, F.; Trogler, W. C.; Ernst, R. D. *J. Am. Chem. Soc.* **1986**, *108*, 6046. (e) Kowaleski, R. M.; Rheingold, A. L.; Trogler, W. C.; Basolo, F. *Ibid.* **1986**, *108*, 2460.

(8) Downard, A. J.; Robinson, B. H.; Simpson, J. *Organometallics* **1986**, *5*, 1140.

(9) (a) Okuhara, K. *J. Am. Chem. Soc.* **1980**, *102*, 244. (b) Lawrence, L. M.; Whitesides, G. M. *Ibid.* **1980**, *102*, 2493. (c) Ashby, E. C.; Bowers, J. R., Jr. *Ibid.* **1981**, *103*, 2242. (d) Poë, A.; Sekbar, C. V. *Ibid.* **1985**, *107*, 4874.

(10) Natalyia, N. N.; Huggins, J. M. *Organometallics* **1986**, *5*, 1703.

(11) Herrinton, T. R.; Brown, T. L. *J. Am. Chem. Soc.* **1985**, *107*, 5700.

(12) (a) Bagchi, R. N.; Bond, A. M.; Colton, R.; Luscombe, D. L.; Moir, J. E. *J. Am. Chem. Soc.* **1986**, *108*, 3352. (b) Bond, A. M.; Colton, R.; McGregor, K. *Inorg. Chem.* **1986**, *25*, 2378.

(13) (a) Wrighton, M. S.; Ginley, D. S. *J. Am. Chem. Soc.* **1975**, *97*, 2065. (b) Hepp, A. F.; Wrighton, M. S. *Ibid.* **1983**, *105*, 5935. (c) Hepp, A. F.; Wrighton, M. S. *Ibid.* **1981**, *103*, 1258.

(14) Doxsee, K. M.; Grubbs, R. H.; Anson, F. C. *J. Am. Chem. Soc.* **1984**, *106*, 7819. Note the difference from the proposed role of the nucleophile in catalysis of migratory insertion of carbon monoxide in 18e systems as in the following: Webb, S. L.; Giandomenico, C. M.; Halpern, J. *J. Am. Chem. Soc.* **1986**, *108*, 345. Wax, M. J.; Bergman, R. G. *Ibid.* **1981**, *103*, 7028. Mawby, R. J.; Basolo, F.; Pearson, R. G. *Ibid.* **1964**, *86*, 3994.

(15) Narayanan, B. A.; Kochi, J. K. *J. Organomet. Chem.* **1984**, *272*, C49.

(16) Krusic, P. J.; Briere, R.; Rey, P. *Organometallics* **1985**, *4*, 801.

(17) Therien, M. J.; Ni, C.-L.; Anson, F. C.; Osteryoung, J. G.; Trogler, W. C. *J. Am. Chem. Soc.* **1986**, *108*, 4037.

(18) (a) Magnuson, R. H.; Zulu, S.; T'sai, W.-M.; Giering, W. P. *J. Am. Chem. Soc.* **1980**, *102*, 6887. (b) Magnuson, R. H.; Meirowitz, R.; Zulu, S.; Giering, W. P. *Ibid.* **1982**, *104*, 5790. (c) Magnuson, R. H.; Meirowitz, R.; Zulu, S. J.; Giering, W. P. *Organometallics* **1983**, *2*, 460.

(19) (a) Feder, H. M.; Halpern, J. *J. Am. Chem. Soc.* **1975**, *97*, 7187. (b) Sweany, R.; Halpern, J. *Ibid.* **1977**, *99*, 8335.

(20) (a) Rathke, J. W.; Feder, H. M. *J. Am. Chem. Soc.* **1978**, *100*, 3623. (b) Azran, J.; Orchin, M. *Organometallics* **1984**, *3*, 197.

(21) (a) Anderson, S. N.; Fong, C. W.; Johnson, M. D. *J. Chem. Soc., Chem. Commun.* **1973**, 163. (b) Nicholas, K. M.; Rosenblum, M. *J. Am. Chem. Soc.* **1973**, *95*, 4449. (c) Bock, P. L.; Boschetto, D. J.; Rasmussen, J. R.; Demers, J. P.; Whitesides, G. M. *Ibid.* **1974**, *96*, 2814. (d) LaCroce, S. J.; Cutler, A. R. *Ibid.* **1982**, *104*, 2312. (e) Cameron, A.; Smith, V. H.; Baird, M. C. *Organometallics* **1983**, *2*, 465. (f) Bly, R. S.; Silverman, G. S.; Bly, R. K. *Ibid.* **1985**, *4*, 374. (g) Reger, D. L.; Mintz, E. *Ibid.* **1984**, *3*, 1759. (h) Reger, D. L.; Mintz, E.; Lebioda, L. *J. Am. Chem. Soc.* **1986**, *108*, 1940.

0002-7863/87/1509-5127$01.50/0 © 1987 American Chemical Society

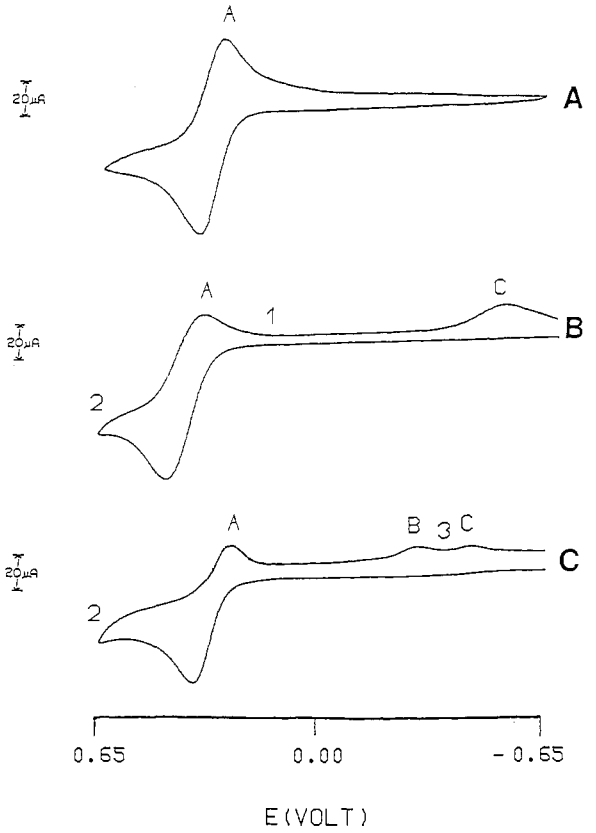

Figure 1. (A) Cyclic voltammogram at 20 °C showing the redox couple for $CpFe(CO)(PPh_3)CH_3^{0/+}$ ($E_{1/2}$ = 325 mV; labeled A). Experimental conditions: $[CpFe(CO)(PPh_3)CH_3]$ = 1 × 10^{-3} M, [TBAHFP] = 0.15 M, solvent = CH_2Cl_2, potentials relative to an Ag wire pseudoreference electrode ($E_{1/2}$(ferrocene) = 330 mV), scan rate = 200 mV/s. TBAHFP = tetra-*n*-butylammonium hexafluorophosphate. (B) Cyclic voltammogram at 20 °C showing the redox couple for $CpFe(CO)(PPh_3)CH_3^{0/+}$ (labeled A) and the cathodic wave corresponding to the reduction of $CpFe(PPh_3)(py)(COCH_3)^+$ (E_{pc} = −490 mV; labeled C). Experimental conditions: same as above except [py] = 30 × 10^{-3} M. (C) Cyclic voltammogram at 0 °C that shows, in addition to redox couple A and cathodic wave C, an intermediate reduction wave (E_{pc} = −290 mV, labeled B). Experimental conditions: same as above except [py] = 200 × 10^{-3} M.

in coordination sphere expansion and formation of a hypervalent 19e intermediate or transition state. The transient electrochemical techniques used in this study permit the determination of rate constants for nucleophilic attack at the 17e metal center and for the alkyl-to-acyl migratory insertion.

Results and Discussion

Qualitative Electrochemical Studies. Our electrochemical studies of the oxidatively induced carbonyl insertion reaction center on $CpFe(CO)(PPh_3)CH_3$, a compound used previously to establish electrocatalyzed CO insertion.[18] This complex undergoes a reversible one-electron oxidation, $E_{1/2}$ = 325 mV (relative to an Ag wire pseudoreference electrode; $E_{1/2}$(ferrocene) = 330 mV) in CH_2Cl_2 (Figure 1A) at 20 °C. Addition of a 30-fold molar excess of pyridine to the electrochemical cell results in the cyclic voltammogram (scan rate = 200 mV/s) shown in Figure 1B. Similar to that reported in acetonitrile,[18] this voltammogram exhibits the redox couple for $CpFe(CO)(PPh_3)CH_3^{0/+}$ ($E_{1/2}$ = 325 mV, denoted A) and the reduction wave for $CpFe(PPh_3)(py)(COCH_3)^+$ (E_{pc} = −490 mV, denoted C), the product of migratory insertion. On cooling the cell to 0 °C, the iron–alkyl redox couple becomes chemically reversible. Increasing the pyridine concentration from a 30 to a 200 molar excess produces the voltammetric response shown in Figure 1C. Note the appearance of a new reduction wave (labeled B) at −290 mV, well before the potential required to reduce the 17e acyl cation.

Cathodic wave B can also be observed at room temperature for fast scan rates (ν) (Figure 2). Addition of a 30-fold excess

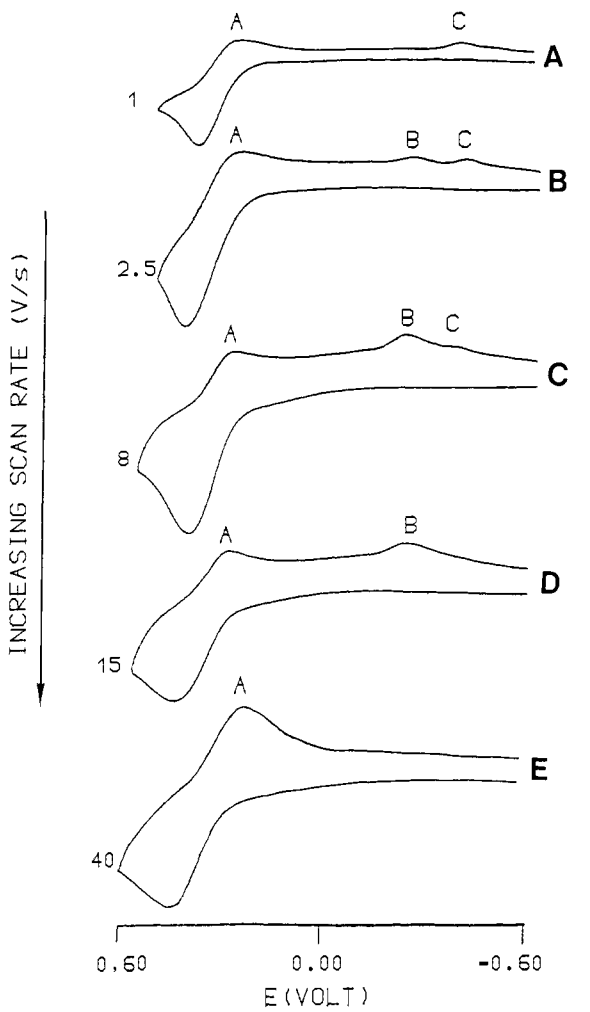

Figure 2. A series of cyclic voltammograms showing the relationship between scan rate and the species observed electrochemically for the alkyl-to-acyl migratory insertion reaction at 20 °C. Experimental conditions: $[CpFe(CO)(PPh_3)CH_3]$ = 1 × 10^{-3} M, [TBAHFP] = 0.15 M, [3,4-$(Me)_2$-py] = 20 × 10^{-3} M, solvent = CH_2Cl_2. Labeling scheme: same as Figure 1. Scan rates: (A) 1 V/s, (B) 2.5 V/s, (C) 8 V/s, (D) 15 V/s, (E) 40 V/s.

of 3,4-dimethylpyridine (3,4-lutidine) to a 1 × 10^{-3} M solution of $CpFe(CO)(PPh_3)CH_3$ in CH_2Cl_2 produces the cyclic voltammetric response shown in Figure 2A (ν = 1 V/s). Similar to Figure 1B, the cyclic voltammogram shows only redox couple A and cathodic wave C. Increasing the scan rate to 2.5 V/s (Figure 2B) shows the new species (B) and the acyl species (C) present in about equal concentrations. At 8 V/s (Figure 2C), the amount of the new species B increases while there is a concomitant decrease in the acyl species (C). At 15 V/s (Figure 2D) only redox couple A and cathodic wave B remain. Even at a scan rate of 15 V/s, repeated cyclic voltammograms show no anodic couple for cathodic wave B. Increasing the scan rate to 40 V/s (Figure 2E) results in a voltammetric response showing only the redox couple for $CpFe(CO)(PPh_3)CH_3^{0/+}$ (A). Whatever species B, these experiments suggest that it is an intermediate along the carbonyl insertion pathway.

Further cyclic voltammetric studies are shown in Figure 3, which compare the responses observed when nitrogen donors of differing σ-basicities are added to solutions of $CpFe(CO)(PPh_3)CH_3$ before the initial anodic scan. Column II of this figure shows the cyclic voltammograms observed on generating $CpFe(CO)(PPh_3)CH_3^+$ in the presence of a 200-fold molar excess of pyridine at three different scan rates. Similar to results in Figure 2, increasing the scan rate increases the amount of species B and decreases the acyl species (labeled C) present. Columns I and III shows that other nucleophiles such as 3,4-dimethylpyridine (60-fold molar excess) or 3-chloropyridine (5000-fold molar ex-

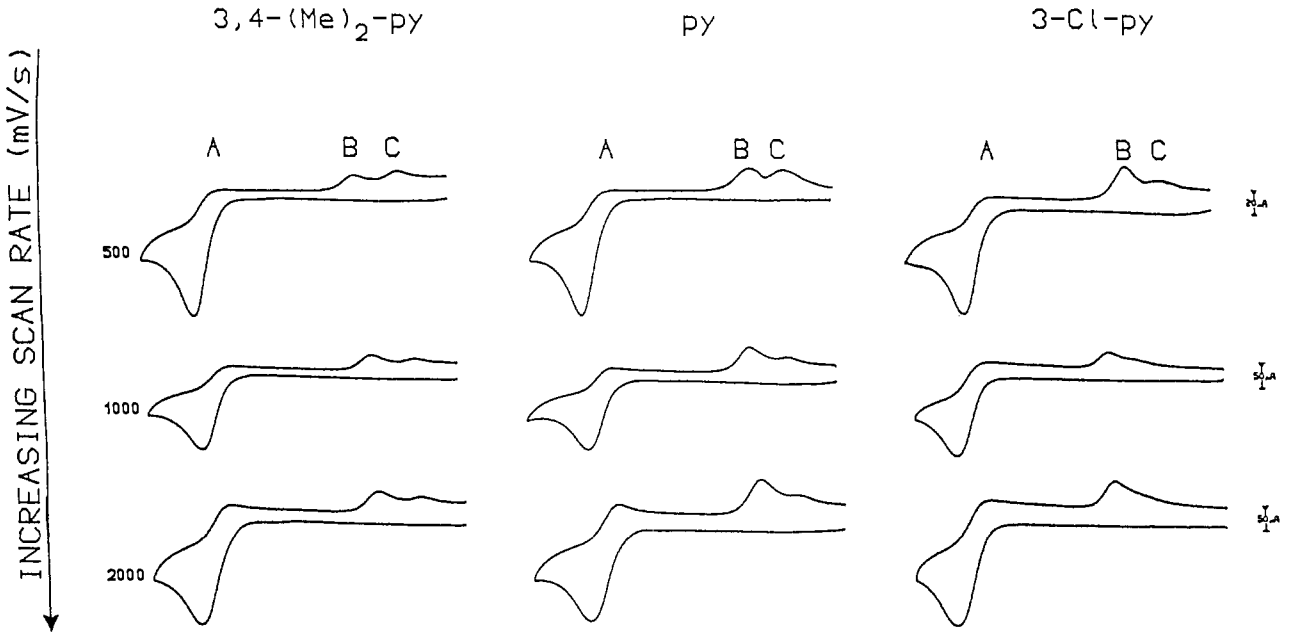

Figure 3. A matrix of cyclic voltammograms showing the relationship between the nucleophile used, scan rate, and the species observed electrochemically for the insertion reaction at 0 °C. Column I depicts the responses observed for [3,4-$(Me)_2$-py] = 60×10^{-3} M at three different scan rates, while columns II and III respectively show the responses for [py] = 480×10^{-3} M and [3-Cl-py] = 7500×10^{-3} M at identical scan rates. Experimental conditions: [$CpFe(CO)(PPh_3)CH_3$] = 1×10^{-3} M, [TBAHFP] = 0.15 M, solvent = CH_2Cl_2.

cess), respectively, give similar results. The concentrations of these ligands were adjusted to give a similar current for reduction of $CpFe(CO)(PPh_3)CH_3^+$ (A) at a given scan rate. Stabilization of species B by excess nucleophile suggests it is an adduct that contains bound nucleophile.

It is now well known[3,5-8,12-17] that many 17e organometallics undego substitution via associative pathways to produce 19e intermediates or transition states and that nucleophilic attack is accelerated by 10^9-fold at 17e iron centers[17] as compared to their 18e analogues. The observation that increased amounts of nucleophile are required to promote migratory insertion as the nucleophile becomes less electron rich is consistent with an associative mechanism and our previous studies involving attack at iron carbonyl cation radicals.[17] The scan rate dependencies shown in Figure 2 suggest species B forms before migratory insertion occurs. For a constant scan rate the increase in the B:C ratio observed for less electron rich nucleophiles suggests the 19e intermediate inserts CO more slowly for poor nucleophiles. We formulate this intermediate as $CpFe(CO)(PPh_3)(Nu)CH_3^+$ (where Nu = substituted pyridine) and propose that the reduction at cathodic wave B in Figure 2 corresponds to

$$CpFe(CO)(PPh_3)(Nu)CH_3^+ + e^- \rightleftharpoons CpFe(CO)(PPh_3)CH_3 + Nu \quad (3)$$

The data support a mechanism for migratory insertion shown in Scheme I and rule out a mechanism where insertion occurs before coordination of nucleophile to give a 15e intermediate.

IR, Electrochemical, and EPR Characterization of the 19-Electron Intermediate. In situ oxidation of $CpFe(CO)(PPh_3)CH_3$ (ν_{CO} = 1904 cm^{-1}) with 1 equiv of $AgPF_6$ in CH_2Cl_2 solvent results in clean conversion to $[CpFe(CO)(PPh_3)CH_3][PF_6]$ (ν_{CO} = 1966 cm^{-1}). Addition of 200 equiv of pyridine-d_5 at low temperature (ca. −40 °C) results in the immediate formation of a new CO-containing species ν_{CO} = 1916 cm^{-1} that appears to be in equilibrium with the alkyl cation. The high value of ν_{CO} proves that insertion has not occurred in the intermediate. Slow formation of the acyl cation (ν_{CO} = 1645 cm^{-1}), the product of the migratory insertion, then occurs.

Formulation of the new CO-containing species as a 19e intermediate seems reasonable since ν_{CO} lies between the neutral and cationic iron–alkyl complexes. On the basis of the red-shifted infrared absorption at 1916 cm^{-1}, it could also be argued that species B arises from the substitution of PPh_3 in $CpFe(CO)(PPh_3)CH_3^+$ to give 17e $CpFe(CO)(py)CH_3^+$.[22] If this structure

Scheme I

$$CpFe(CO)(PPh_3)CH_3 \underset{+e^-}{\overset{-e^-}{\rightleftharpoons}} CpFe(CO)(PPh_3)CH_3^+ \quad (4)$$
18e 17e

$$CpFe(CO)(PPh_3)CH_3^+ + Nu \underset{k_{-2}}{\overset{k_1}{\rightleftharpoons}} CpFe(CO)(PPh_3)(Nu)CH_3^+ \quad (5)$$
17e 19e

$$CpFe(CO)(PPh_3)(Nu)CH_3^+ \underset{k_{-2}}{\overset{k_2}{\rightleftharpoons}} CpFe(Nu)(PPh_3)(COCH_3)^+ \quad (6)$$
19e 17e

were the correct formulation of B, then it would not be a direct antecedent of the acyl product C and would necessarily be in equilibrium with $CpFe(CO)(PPh_3)CH_3^+$ or a "true" 19e intermediate, which we do not observe.

To test if pyridine partially displaces triphenylphosphine in $CpFe(CO)(PPh_3)CH_3^+$ to form B, 250 equiv of PPh_3 were added to a solution of $CpFe(CO)(PPh_3)CH_3$ before the initial anodic scan cyclic voltammogram under the experimental conditions described for Figure 1A. The cyclic voltammetric response obtained was *identical* with that shown in Figure 1A, a reversible redox couple with $E_{1/2}$ = 325 mV. This shows that PPh_3 does not promote the oxidatively induced insertion reaction on the time scales of these cyclic voltammetric experiments. Addition of 30 equiv of pyridine (relative to $CpFe(CO)(PPh_3)CH_3$) to this solution results in a cyclic voltammogram *identical* with that shown in Figure 1B, which proves that excess PPh_3 does not inhibit the pyridine-induced insertion reaction. Cooling this solution in the electrochemical cell to 0 °C and increasing the pyridine con-

(22) (a) A referee has suggested an alternative structure for species B that results from pyridine nucleophile binding reversibly to the cyclopentadienyl ring of $CpFe(CO)(PPh_3)CH_3^+$. Although we cannot rule out such a complex, we point out that while such arene ring adducts are known[22b-d], there is little precedent for such species involving cyclopentadienyl rings. Previous studies of substitution at cyclopentadienyl metal radicals[3,6,10] show no evidence for such species regardless of the type of nucleophile used. Moreover, of the complexes of this type that are known, the ring adducts form with charged species such as hydride. Finally, the Hammett ρ value obtained in our system is consistent with nucleophile attack at a metal radical center.[3c,17] Such large negative values of ρ are unusual for nucleophilic attack at carbon. Thus we do not view this alternative as likely. (b) Kane-Maguire, L. A. P.; Sweigart, D. A. *Inorg. Chem.* **1979**, *18*, 700. (c) Winkhaus, G.; Pratt, L.; Wilkinson, G. *J. Chem. Soc.* **1961**, 3807. (d) Jones, D.; Pratt, L.; Wilkinson, G. *J. Chem. Soc.* **1962**, 4458.

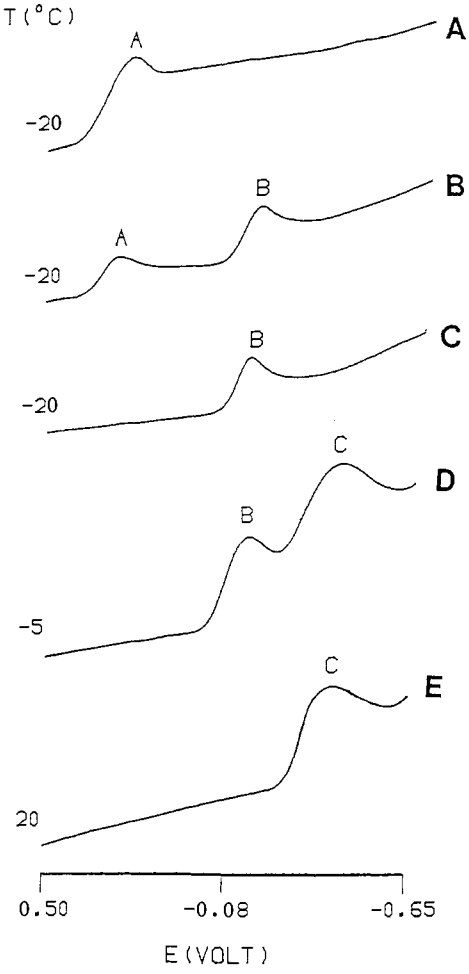

Figure 4. A series of linear sweep voltammograms at three different temperatures showing that chemically generated $CpFe(CO)(PPh_3)CH_3^+$ converts to the acyl insertion product, $CpFe(PPh_3)(py)(COCH_3)^+$, via intermediate species B = $CpFe(CO)(PPh_3)(py)CH_3^+$. Experimental conditions: $[CpFe(CO)(PPh_3)CH_3][PF_6] = 1 \times 10^{-3}$ M, [TBAHFP] = 0.15 M, solvent = CH_2Cl_2, temperatures as labeled. Nucleophile concentrations: (A) [py] = 0, (B) [py] = 200×10^{-3} M, (C) [py] = 400×10^{-3} M, (D) [py] = 400×10^{-3} M, (E) 400×10^{-3} M.

centration to give a 200-fold molar excess (experimental conditions identical with those for Figure 1C, except for added PPh_3) produced a cyclic voltammogram *identical* with that in Figure 1C. Voltammetric responses at increased scan rates were also identical with those depicted in column II of Figure 3. Addition of another 250 equiv of PPh_3 to this solution did not alter the cyclic voltammetric responses described in the above discussion. These findings conclusively show that species B does not result from phosphine substitution by pyridine since the excess phosphine present would assuredly affect the equilibrium concentration of a species formed by loss of phosphine, and thereby the acyl product C. These results are in accord with what is known[1-7,11,17] about substitution processes at 17e metal radicals; phosphine ligands are not displaced at electron-deficient metal centers when CO ligands are present.

Addition of 1 equiv of $AgPF_6$ to $CpFe(CO)(PPh_3)CH_3$ gives the 17e complex $[CpFe(CO)(PPh_3)CH_3][PF_6]$. A linear sweep voltammogram of chemically generated $CpFe(CO)(PPh_3)CH_3^+$ shows the expected cathodic response (E_{pc} = 275 m V) corresponding to the one-electron reduction that yields $CpFe(CO)(PPh_3)CH_3$ at the electrode surface. Addition of 200 equiv of pyridine to the solution results in the linear sweep voltammogram of Figure 4B. A second cathodic wave is observed (E_{pc} = −290 mV) corresponding to the proposed 19e complex B. The estimated equilibrium constant for its formation is ~7. Addition of 200 more equivalents of pyridine drives all the material in the bulk phase of the solution to species B (Figure 4C). Warming this solution quickly to −5 °C gives the cathodic scan linear sweep voltammogram of Figure 4D, which shows only the presence of the intermediate B and the acyl species C. After this solution was warmed quickly to 20 °C, the linear sweep voltammogram obtained (Figure 4E) showed only species C, the product of alkyl-to-acyl migratory insertion.

This technique could not be used to measure the rate of alkyl-to-acyl migratory insertion since it was observed that even at a low temperature (−20 °C) solutions consisting exclusively of the intermediate B gave linear sweep voltammograms in which the cathodic current associated with the reduction of species B gradually diminished over several minutes. The decomposition of the intermediate B most likely arises from a disproportionation pathway common for radical species.[6,7,17] This experiment further supports the hypothesis that B is an intermediate along the carbonyl insertion pathway and a *direct antecedent* of the acyl species C.

In addition, the EPR spectra of chemically generated $CpFe(CO)(PPh_3)CH_3^+$ at −20 °C show a doublet (g = 2.009, a(P) = 120 G) as expected for coupling of the unpaired electron spin to the phosphorus atom of the phosphine. Spectra (−20 °C) of species B, generated under experimental conditions identical with those of Figure 4C, show a doublet similar to that observed for the parent cation (g = 2.000, a(P) = 120 G). Thus the IR experiments show CO remains bound to iron in species B. The cyclic and linear sweep voltammetric studies show PPh_3 remains bound to iron in the intermediate B, which is further confirmed by the EPR results.

Kinetic Analysis of the Alkyl-to-Acyl Migratory Insertion Reation. Transient electrochemical techniques such as double potential step chronocoulometry (DPSCC)[23] aid in the study of rapid chemical reactions that are coupled to electrode reactions and can provide information about reaction rates and mechanisms.[3,14,17,24] The double potential step experiment consists of stepping the potential from an initial value, E_i (labeled 1 in Figure 1B), where no electrode reaction proceeds, to a final value, E_f (labeled 2), where the species of kinetic interest, 17-electron $CpFe(CO)(PPh_3)CH_3^+$, forms at the electrode surface. After holding the potential at E_f for a time, τ, it is stepped back to E_i and maintained there for the same interval τ. During this period a portion of the 17e cation radical generated at E_f is converted back to starting material ($CpFe(CO)(PPh_3)CH_3$). The charge that passes through the electrode during each time interval is measured. The ratio of the reverse (Q_R) to forward (Q_F) charge provides a measure (after correction for background contributions in blank experiments) of the chemical reactions that consume $CpFe(CO)(PPh_3)CH_3^+$ generated at E_f. In the absence of a nitrogen Lewis base the charge ratio Q_R/Q_F was within 2% of the expected value of 0.586[23] for a chemically reversible redox couple and independent of step duration, τ. The reaction pathway outlined in Scheme I for the alkyl-to-acyl migratory insertion corresponds to an ECC mechanism, i.e., an electrode reaction (E) followed by two successive chemical reactions (CC). When both chemical reactions can be regarded as irreversible, analysis of the kinetic parameters by double potential step methods is straightforward.[24] The cyclic voltammetric responses observed for the alkyl-to-acyl migratory insertion do not require k_{-1} and k_{-2} to be negligible as compared to k_1 and k_2, respectively. Fortunately, the chemistry observed in this system possesses features that allow measurement of the rate constants with double potential step chronocoulometry.

Since cathodic wave B is not observed at 20 °C (Figure 1B), this shows that the 19e intermediate, $CpFe(CO)(PPh_3)(py)CH_3^+$, obeys steady state control for low nucleophile concentrations and moderately fast scan rates.[25] Thus, a double potential step

(23) (a) Christie, J. H.; Anson, F. C.; Lauer, G.; Osteryoung, R. A. *Anal. Chem.* **1963**, *35*, 1979. (b) Bard, A. J.; Faulkner, L. R. *Electrochemical Methods*; John Wiley and Sons: New York, 1980. (c) Christie, J. H.; Osteryoung, R. A.; Anson, F. C. *J. Electroanal. Chem.* **1967**, *13*, 236. (d) Christie, J. H. *Ibid.* **1967**, *13*, 79. (e) Anson, F. C. *Acc. Chem. Res.* **1975** *18*, 400 and references therein.

(24) Hanafey, M. K.; Scott, R. L.; Ridgway, T. H.; Reilley, C. N. *Anal. Chem.* **1978**, *50*, 116 and references therein.

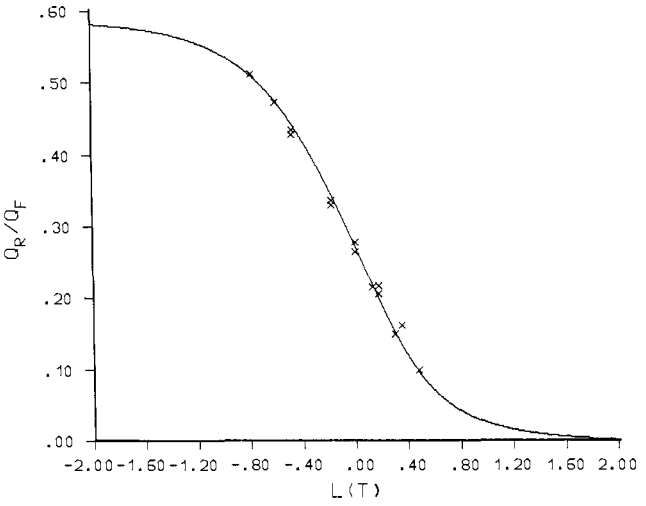

Figure 5. Variation of the charge ratio, Q_R/Q_F, with the parameter $L(T) = \log (k_1[Nu]\tau)$ for an EC mechanism where the value of $k_{-1}/k_1[Nu]$ equals zero. The solid line represents the theoretical working curve for the mechanism and the crosses the experimental responses obtained at nucleophile concentrations between 10 and 90 mM and pulse widths τ between 250 and 1000 ms. Experimental systems: $[CpFe(CO)(PPh_3)CH_3] = 1 \times 10^{-3}$ M, [TBAHFP] = 0.15 M, temperature = 20 °C, solvent = CH_2Cl_2, E_i = 100 mV, E_f = 600 mV (potentials relative to a silver wire pseudoreference electrode, $E_{1/2}$(ferrocene) = 330 mV), [Nu] = pyridine, and k_1(evaluated) = 33.8 ± 2.4 M^{-1} s^{-1}.

experiment where the initial potential, E_i (labeled 1), and final potential, E_f (labeled 2), are chosen as in Figure 1B should yield charge ratio data consistent with a standard EC mechanistic scheme, even though the reaction follows an ECC pathway. This treatment allows evaluation of the apparent rate constants, k_1^{ap} and k_{-1}^{ap}, defined in eq 7 and 8. At 0 °C, it is possible to adjust

$$k_1^{ap} = k_1k_2/k_{-1} + k_2 \quad (7)$$

$$k_{-1}^{ap} = k_{-1}k_{-2}/k_{-1} + k_{-2} \quad (8)$$

the nucleophile concentration to make redox couple A irreversible. Only waves B and C are observed on the return cathodic voltammetric scan (Figure 3). A double potential step experiment where the initial potential, E_i (labeled 3), and the final potential, E_f (labeled 2), are chosen as in Figure 1C yields charge ratio data that should be consistent with an EC mechanism. This experiment allows evaluation of the rate constants for the alkyl-to-acyl migration (eq 6). The overall ECC reaction pathway is thus broken down into two EC schemes. Working curves for the EC mechanism that plot the expected value of the charge ratio, Q_R/Q_F, as a function of the dimensionless kinetic parameter $k_1\tau$ are available[24] for various values of k_{-1}/k_1.

Double potential step chronocoulometry experiments at 20 °C, with pyridine as the nucleophile to determine the kinetic parameters governing the initial nucleophilic attack by nitrogen Lewis base at the metal center (Scheme I, eq 5), show that the charge ratios obtained decrease with increasing pulse width τ and increasing pyridine concentration. The ratio Q_R/Q_F approaches zero at moderate nucleophile concentrations and long pulse widths. Such behavior requires $k_{-1}^{ap}/k_1^{ap}[Nu] < 10^{-2}$. Otherwise a lower limit to Q_R/Q_F would be observed, because k_{-1}^{ap} produces an electroactive species ($CpFe(CO)(PPh_3)CH_3$) during the reverse step of the experiment, which would give a measurable value of Q_R. Figure 5 shows the experimental values of Q_R/Q_F, obtained at five different nucleophile concentrations fit to the working curve for an EC mechanism, where the parameter $k_{-1}^{ap}/k_1^{ap}[Nu] = 0$. This special case of the EC mechanism is often referred to as EC_i.

(25) As seen in Figure 2, extremely fast scans at 20 °C allow the 19e intermediate (cathodic wave B) to build up along the carbonyl insertion pathway. This result does not complicate our kinetic analysis since the step durations (τ) used in the DPSCC experiments correspond to scan rates less than 500 mV/s.[22b]

Table I. Rate Constants[a] for Nucleophilic Attack at $CpFe(CO)(PPh_3)CH_3^+$ by Substituted Pyridines at 20 °C.

nucleophile	k_1 (M^{-1} s^{-1})	nucleophile	k_1 (M^{-1} s^{-1})
3,4-dimethylpyridine	200	3-fluoropyridine	0.27
4-methylpyridine	105	3-chloropyridine	0.14
3-methylpyridine	93.7	4-cyanopyridine	0.10
pyridine	33.8 ± 2.4[b]	3-cyanopyridine	0.04

[a] Experimental conditions: $[CpFe(CO)(PPh_3)CH_3] = 1 \times 10^{-3}$ M, TBAHFP = 0.15 M, solvent = CH_2Cl_2, temperature = 20 °C, E_i = 100 mV, E_f = 600 mV (potentials relative to a silver wire pseudoreference electrode, $E_{1/2}$(ferrocene) = 330 mV). [b] Rate constants for all nucleophiles were measured from the fit of experimental double potential step chronocoulometry charge response ratios to an EC_i mechanism. Standard deviations in the measured rate constants for the 3- and 4-substituted pyridine should be similar to that observed for pyridine (±7% of the reported value).

Table II. Observed Rate[a] Dependencies for Nucleophilic Attack[b,c] at $CpFe(CO)(PPh_3)CH_3^+$ in CH_2Cl_2 at 20 °C

k_{obsd}	[nucleophile] (mM)	k_{obsd}	[nucleophile] (mM)
0.34	10	2.00	60
0.72	20	3.09	90
1.41	40		

[a] Measured with double potential step chronocoulometry; rates reported are the average of the values obtained at the different experimental pulse widths. Experimental conditions: same as Table I. [b] Nucleophile = pyridine. [c] k_1 = 33.8 ± 2.4 M^{-1} s^{-1}.

Table III. Data Used for Hammett Analysis of the Rate of Nucleophilic Attack at $CpFe(CO)(PPh_3)CH_3^+$ by 3- and 4-Substituted Pyridines[a]

nucleophile	log k_1	pK_a[b]	$\sigma_{m,p}$[c]
3,4-dimethylpyridine	2.30	6.48	−0.21
4-methylpyridine	2.02	6.03	−0.14
3-methylpyridine	1.97	5.67	−0.08
pyridine	1.52	5.21	0.00
3-fluoropyridine	−0.57	3.02	0.36[d]
3-chloropyridine	−0.85	2.81	0.40
4-cyanopyridine	−1.00	1.86	0.55
3-cyanopyridine	−1.40	1.35	0.64

[a] Experimental conditions: same as Table I. [b] pK_a of the pyridinium/pyridine couple in H_2O (from ref 26). [c] The use of these values in this non-aqueous system is justified by the fact that the trend of pK_a's of substituted pyridines is known to be the same in aprotic solvents (ref 26c). Gas-phase and aqueous values are compared in ref 26d. [d] Estimated from ref 26.

Although the experimental data will fit any EC working curve where $0 \le k_{-1}^{ap}/k_1^{ap}[Nu] \le 10^{-2}$, the data suggest that $k_{-1}^{ap} \approx 0$ and hence $k_{-1} = 0$ and $k_1^{ap} = k_1$. The second-order rate constant, k_1, for nucleophilic attack at 17e $CpFe(CO)(PPh_3)CH_3^+$ was determined to be 33.8 ± 2.4 M^{-1} s^{-1} (Table I). A plot of k_{obsd} vs. nucleophile concentration (Table II) shows a first-order dependence on incoming nucleophile. Since no nucleophile-independent pathway exists under the experimental conditions, this establishes a second-order rate law (eq 9).

$$-d[CpFe(CO)(PPh_3)CH_3^+]/dt = k_1[CpFe(CO)(PPh_3)CH_3^+][Nu] \quad (9)$$

Electronic Effects on Nucleophilic Attack. By using the electrochemical techniques discussed, the second-order rate constants k_1 were determined for a series of 3- and 4-substituted pyridines (Table I) at 20 °C. The pK_a's, log k_1's, and the Hammett σ-meta and σ-para values[26] for the 3- and 4-substituted pyridines are compared in Table III. The negative slope (or sign of ρ) in the Hammett plot of Figure 6 shows that the transition state formed via nucleophilic attack must be favored by increased electron donation to the frontier orbital of the pyridine base, while the large

(26) (a) Fisher, A.; Galloway, W. J.; Vaughan, J. *J. Chem. Soc.* **1965**, 3591. (b) Henderson, W. A., Jr.; Streuli, C. A. *J. Am. Chem. Soc.* **1960**, *82*, 5791. (c) Clauguis, G.; Deronzier, A.; Serve, D.; Vieil, E. *J. Electroanal. Chem.* **1975**, *60*, 205. (d) Taagepera, M.; Henderson, W. G.; Brownless, R. T.; Beauchamp, J. L.; Taft, R. W. *J. Am. Chem. Soc.* **1972**, *94*, 1369.

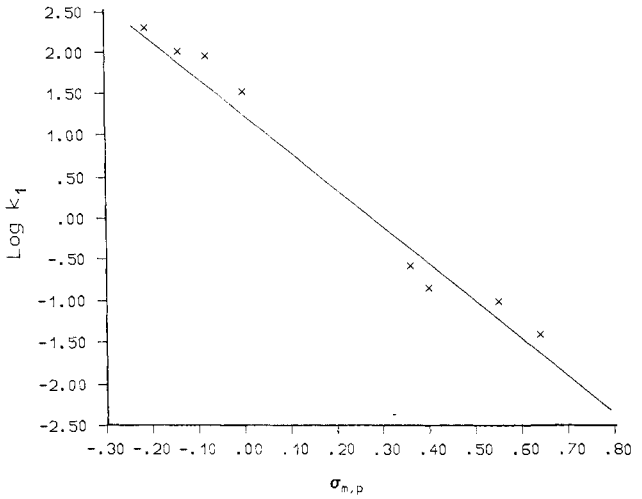

Figure 6. Hammett plot for the meta and para substituent effects on the rate of nucleophilic attack at $CpFe(CO)(PPh_3)CH_3^+$ at 20 °C (see Table III).

value of ρ (−4.69) implies substantial redistribution of charge in the transition state. The value of ρ obtained in this study closely resembles that obtained previously (ρ = −3.25) for associative substitution at iron in another 17e iron complex, $Fe(CO)_3L_2^+$.[17] Both observations support S_N2 attack on iron as the initial chemical step of the carbonyl-insertion reaction.

Although our study agrees with earlier work of Giering and co-workers,[18] which showed that rapid oxidatively induced carbonyl insertion offers a tremendous increase in the equilibrium constant for the alkyl-to-acyl migration in comparison to the neutral 18e complexes, the reported magnitudes of the rate constants involved in the alkyl-to-acyl migration differ considerably. Giering and co-workers[18] place a *lower limit* on the observed rate of oxidatively induced conversion of alkyl to acyl of 100 s^{-1} at 0 °C. Since our study shows that the rate of production of the intermediate that reacts to form the acyl product depends strongly on the electronic features of added nucleophile, we might expect that the poor σ donor acetonitrile ($pK_a \sim -7$) used in the earlier study would react more slowly with $CpFe(CO)(PPh_3)CH_3^+$ than the pyridine-based nucleophiles. That it does not is puzzling. Giering's voltammetric data for this system were obtained in acetone. We have checked the behavior in dichloromethane and its agrees with Giering's results.

In contrast to the kinetic data obtained for the pyridine nucleophiles, which suggests an EC_iC_i mechanism for the oxidatively induced insertion, data obtained for acetonitrile imply that the alkyl-to-acyl migration occurs by an E_rC_r pathway.[18] Perhaps the fast rate observed with acetonitrile results because it is a sterically unhindered ligand and eases strain in the associative transition state. The reversible behavior simply reflects an unfavorable equilibrium.[18c]

Kinetic Parameters of the Insertion Step. Double potential step chronocoulometry experiments at 0 °C, designed to determine the kinetic parameters of the insertion step (Scheme I, eq 6), show that the charge ratios decrease only with increasing step duration τ. Other DPSCC studies with 3,4-dimethylpyridine and pyridine nucleophiles show that the charge ratios measured for the potential step labeled in Figure 1C remain essentially constant at a given pulse width τ as the concentration of nucleophile varies over a wide range (75- to 1000-fold molar excesses). These results suggest that a nucleophilic concentration independent chemical reaction consumes the proposed 19e intermediate, $CpFe(CO)(PPh_3)(Nu)CH_3^+$, as described by eq 6 of Scheme I.

Figure 7 shows the fit of experimental values of Q_R/Q_F obtained for 3-chloropyridine,[27] pyridine, and 3,4-dimethylpyridine nucleohile to the working curve for the EC_i mechanism (the parameter $k_{-2}/k_2 = 0$). While the observed rate of alkyl-to-acyl migratory insertion is nucleophile independent, Figure 7 shows that the rate constants for this process depend on the specific nitrogen Lewis base. The smallest values for the charge ratio that can be measured depend on the intermediate that inserts CO the fastest ($CpFe(CO)(PPh_3)(3,4\text{-}Me_2\text{-}py)CH_3^+$) and the longest accessible pulse times in a DPSCC experiment (~1 s). Although the DPSCC data obtained for the alkyl-to-acyl migration do not require $k_{-2}/k_2 = 0$, they require[24] $k_{-2}/k_2 < 0.2$. Since the linear-sweep voltammetry experiments (Figure 4) suggest that the 19e intermediate can be converted entirely to the acyl product, the assumption that k_{-2} is negligible compared to k_2 (at least for the temperature range between 0 and 20 °C) probably holds. Our kinetic data concur with previous studies[18] that show the equilibrium for the oxidatively induced alkyl-to-acyl migratory insertion to lie far to the right.

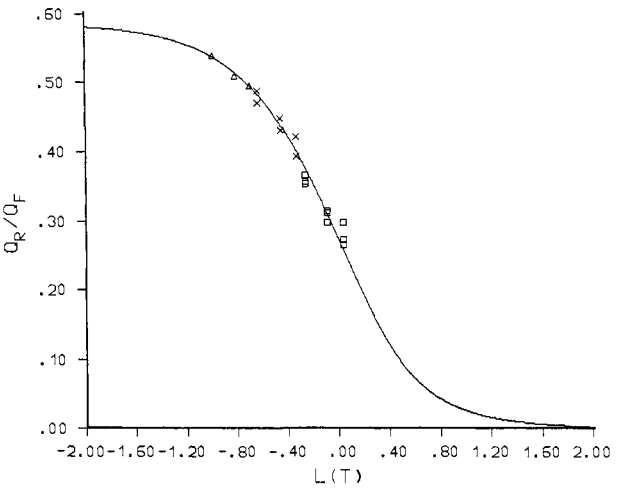

Figure 7. Variation of the charge ratio, Q_R/Q_F, with the parameter $L(T) = \log(k_2\tau)$ for an EC mechanism where the value of $k_{-2}/k_2 = 0$. The solid line represents the theoretical working curve for the mechanism while the triangles, crosses, and boxes represent the experimental data obtained for nucleophiles 3-chloropyridine, pyridine, and 3,4-dimethylpyridine, respectively, at pulse widths τ of 500, 750, and 1000 ms. Experimental system: $[CpFe(CO)(PPh_3)CH_3] = 1 \times 10^{-3}$ M, [TBAHFP] = 0.15 M, temperature = 0 °C, solvent = CH_2Cl_2, E_i = −390 mV, and E_f = 600 mV (potentials relative to a silver wire pseudoreference electrode, $E_{1/2}$(ferrocene) = 330 mV). For the evaluated rate constants, k_2, see Table IV.

Table IV. Rate Constants for the Conversion of $CpFe(CO)(PPh_3)(Nu)CH_3^+$ to $CpFe(PPh_3)(Nu)(COCH_3)^+$ and Nucleophilic Attack of Pyridine at $CpFe(CO)(PPh_3)CH_3^+$ at 0 °C

nucleophile	chemical step	rate constant	k_n
3,4-dimethylpyridine[a]	insertion	k_2 (s^{-1})	1.10 ± 0.12
pyridine[a]	insertion	k_2 (s^{-1})	0.47 ± 0.04
3-chloropyridine[a]	insertion	k_2 (s^{-1})	0.20[c]
pyridine[b]	nucleophilic attack	k_1 (M^{-1} s^{-1})	9.8[c]

[a] Experimental conditions: $[CpFe(CO)(PPh_3)CH_3] = 1 \times 10^{-3}$ M, TBAHFP = 0.15 M, solvent = CH_2Cl_2, temperature = 0.0 °C, E_i = −390 mV (for the pyridine species; the choice of E_i depends on the nucleophile used to generate the $CpFe(CO)(PPh_3)(Nu)CH_3^+$ species), E_f = 600 mV (potentials relative to a silver wire pseudoreference electrode, $E_{1/2}$(ferrocene) = 330 mV). [b] Experimental conditions = same as Table I except temperature = 0.0 °C. [c] Standard deviations were not computed since the rate constants were determined from data obtained at a single nucleophile concentration.

Values of k_2 obtained from the experimental data shown in Figure 7 are displayed in Table IV. The data suggest that the alkyl-to-acyl migration rate depends slightly on the electronic features of the intermediate, with the more electron rich $CpFe(CO)(PPh_3)(Nu)CH_3^+$ species undergoing alkyl-to-acyl migration most rapidly. The rate of the insertion step, however, depends much less on the electronic features of the nucleophile than the associative reaction that produces the 19e intermediate (Table

(27) Only one set of data points was obtained for this nucleophile because of the large amount of Lewis base required (7500-fold molar excess) to drive all the $CpFe(CO)(PPh_3)CH_3^+$ generated at the electrode surface to the intermediate, $CpFe(CO)(PPh_3)(3\text{-}Cl\text{-}py)CH_3^+$.

I). A value of $k_1 = 9.8\ M^{-1}\ s^{-1}$ for L' = pyridine, obtained at low nucleophile concentrations at 0 °C, is included in Table IV.

Summary and Conclusions

Qualitative cyclic voltammetric studies reveal the presence of an intermediate along the carbonyl-insertion pathway in 17e $CpFe(CO)(PPh_3)(CH_3)^+$. Electrochemical and spectroscopic studies show that this species does not arise from simple substitution of phosphine by an entering pyridine nucleophile and is a direct antecedent to the acyl product. All evidence suggests that the intermediate is a hypervalent 19e species of the type $CpFe(CO)(PPh_3)(py)CH_3^+$. Throughout our discussion, the intermediate has been referred to as a 19e species. It is important to point out that an alternative 17e formulation of the intermediate containing a slipped η^3-cyclopentadienyl ring[28,29] is difficult to rule out. In that case, the 19e species discussed would be a transition state instead of an intermediate. We feel, however, there is little need to invoke a slipped ring for the intermediate in the alkyl-to-acyl migratory insertion. The η^5-to-η^3 cyclopentadienyl ring slippage usually occurs when organometallic species wish to avoid 20e rather than 19e configurations.[28,29] Although a 17e slipped indenyl complex is known,[7e] care should be taken regarding extrapolation of this behavior to hypervalent cyclopentadienyl complexes.[30] In addition, the rapid rates of substitution observed in 17e complexes relative to their 18e counterparts[7a,17] have been attributed to two-center–three-electron bonding between the metal and nucleophile. This stabilizes the transition state by formation of a half-order bond to the nucleophile. Just as for 17e complexes, where substitution occurs via 19e intermediates, so too are the 17e acyl products formed from alkyl-to-acyl migration at 19e $CpFe(CO)(PPh_3)(Nu)CH_3^+$. Ring slippage can be viewed as counter productive to the formation of products since hypervalent intermediates appear to be the key in converting 17e species to other, more stable 17e complexes.

Quantitative analysis of the kinetic parameters of the oxidatively induced carbonyl-insertion reaction with double potential step chronocoulometry shows that the overall ECC pathway can be divided into two simple EC_i steps. The data obtained for the first chemical step that produces the hypervalent intermediate is associative in nature; this conclusion is based on (1) the fit of the charge response data to the EC_i mechanism, (2) the effect of increased nucleophile concentration on the observed rate for this conversion, and (3) Hammett analysis of the rate data obtained when the electronic properties of the entering nucleophile are varied. The data obtained for the second chemical step of the sequence, which converts the intermediate to the acyl product, show that it obeys a unimolecular rate law. This conclusion is based on (1) the fit of the charge response data for the EC_i mechanism and (2) the observation that increased nucleophile concentrations do not alter the rate of this conversion.

In conclusion, for the nucleophiles used in this study, the initial chemical step of alkyl-to-acyl migration is associative in nature and the oxidatively induced insertion proceeds via an intermediate of expanded coordination number. *We believe a 17e–19e rule may play a similar role in catalytic cycles for organometallic radicals as the 16e–18e rule*[31] *does in catalytic cycles for closed shell organometallics.*

Experimental Section

Materials. $CpFe(CO)(PPh_3)CH_3$[32] was synthesized by photolysis of $CpFe(CO)_2CH_3$[33] in the presence of 1 equiv of triphenylphosphine in pentane. Various substituted pyridines (Aldrich) (3,4-dimethyl, 4-methyl, 3-methyl, 3-fluoro, and 3-chloro) were degassed and stored over activated molecular sieves (Linde Type 4A) under an inert atmosphere for several days before use. Solid pyridine derivatives 3- and 4-cyanopyridine (Aldrich) were purified by published methods[34] and dried in vacuo. All materials were manipulated by standard Schlenk techniques. Solutions of $CpFe(CO)(PPh_3)CH_3$ were prepared under N_2 in a Vacuum Atmospheres glovebox equipped with a HE-493 Dri-Train.

Electrochemical Studies. The supporting electrolyte (tetra-*n*-butylammonium hexafluorophosphate, Southwestern Chemical, Electrometric Grade) was recrystallized twice from a mixture of ethyl acetate and pentane (Burdick and Jackson) and dried in vacuo. Dichloromethane (analytical reagent, Mallinckrodt) was distilled from CaH_2 under nitrogen and stored under an inert atmosphere in a Schlenk flask. Pyridine (Aldrich Spectrophotometric Grade, Gold Label) was stored over KOH pellets for several days and then distilled twice from BaO under a nitrogen atmosphere. (Other pyridine derivatives were degassed and stored over activated molecular sieves.)

Cyclic voltammetry and double potential step chronocoulometry experiments used a BAS-100 Electrochemical Analyzer interfaced to a BAS Model PL-10 digital plotter. The electrochemical cell consisted of an IBM voltammetric cell assembly equipped with a thermostated jacket. The platinum disk working electrodes and the platinum wire auxiliary electrodes used were obtained from both IBM Instruments and BAS. Temperatures of solutions were measured with a Love digital thermometer (±0.1 °C) calibrated at 0.0 and −78.0 °C. A Brinkman-Lauda RMS constant temperature circulating bath was used to maintain the cell temperature. The solution in the cell was blanketed with nitrogen, presaturated with solvent at the same temperature.

In a typical cyclic voltammetry experiment, 5 mL of a 0.15 M tetra-*n*-butylammonium hexafluorophosphate (TBAHFP) stock solution was syringed into the electrochemical cell and the potential of the working electrode was cycled several times between the initial and final values. Then, 5 mL of a solution 2 mM in $CpFe(CO)(PPh_3)CH_3$ and 0.15 M in TBAHFP was syringed into the cell along with a known concentration of nucleophile (if used). Voltammograms were recorded at several scan rates, with stirring between each measurement. Platinum working and auxiliary electrodes were cleaned with aqua regia after each set of experiments. The platinum working electrode was polished with 0.3-μm alumina. No contamination of the electrode surfaces was observed in the potential window of these experiments. Reproducible cyclic voltammograms were obtained throughout the course of each set of experiments.

Chronocoulometric measurements were conducted under the conditions described above for the cyclic voltammetric measurements. Use of a silver wire pseudoreference electrode avoided the problem of leakage of Ag^+ ions from a solution reference electrode into the test solutions, which lowered the background current. The charge response ratios, Q_R/Q_F, were calculated after correction of both Q_R and Q_F for background contributions in blank experiments. Error limits reported for kinetic parameters represent a single standard deviation from unweighted least-squares analysis.

Spectral Studies. Infrared spectra were recorded with use of an IBM FTIR/32 instrument. EPR spectra were recorded at room temperature and at −20 °C with a Varian E-3 spectrometer. Low-temperature EPR samples were cooled in a dewar via a stream of nitrogen gas (−78 °C). Sample temperature was monitored with an Omega 651 resistance thermometer.

Acknowledgment. This material is based on work supported by the National Science Foundation (Grant CHE-85-04088). We thank Prof. Christian Amatore for helpful discussions. W.C.T. thanks the Alfred P. Sloan Foundation for a research fellowship.

(28) (a) Rerek, M. E.; Basolo, F. *Organometallics* **1983**, *2*, 372. (b) Rerek, M. E.; Basolo, F. *J. Am. Chem. Soc.* **1984**, *106*, 5908. (c) Cramer, R.; Seiwell, L. P. *J. Organomet. Chem.* **1975**, *92*, 245. (d) Bergman, R. G. *Acc. Chem. Res.* **1980**, *13*, 113. (e) Casey, C. P.; O'Connor, J. M.; Haller, K. J. *J. Am. Chem. Soc.* **1985**, *107*, 1241.

(29) For an excellent review, see: O'Connor, J. M.; Casey, C. P. *Chem. Rev.* **1987**, *87*, 307.

(30) Miller, G. A.; Therien, M. J.; Trogler, W. C., submitted.

(31) (a) Tolman, C. A. *Chem. Soc. Rev.* **1972**, *1*, 337. (b) Parshall, G. W. *Homogeneous Catalysis*; Wiley: New York, 1980.

(32) Reger, D. L.; Culbertson, E. C. *Syn. React. Metal-Org. Chem.* **1976**, *6*, 1.

(33) (a) Piper, T. S.; Wilkinson, G. *J. Inorg. Nucl. Chem.* **1956**, *3*, 104. (b) Plotkin, J. S.; Shore, S. G. *Inorg. Chem.* **1981**, *20*, 284.

(34) Perrin, D. D.; Araregó, W. L. F.; Perrin, D. R. *Purification of Laboratory Chemicals*; Pergamon: New York, 1980.